Effect of Frequency Domain Filtering on Fourier Transform Based Phase Extraction

Prafull Padghan[1*], *Pallavi* Nalle[1], *Vaishnavi* Atole[1] and *Kamlesh* Alti[2]

[1]Department of Physics, Shri Shivaji Science and Arts College Chikhli, Dist. Buldhana, Maharashtra, India
[2]Department of Physics, Institute of Science Nagpur, Maharashtra, India

Abstract. Phase extraction from single interference fringe pattern is an essential step in quantitative interferometry measurements particularly in single shot analysis. Fringe pattern obtained from an interferometer often contain noise due to environmental disturbances and imaging limitations which can affect accuracy of phase retrieval. In this work, Fourier transform method is employed for phase extraction from single image of fringe pattern. This method is applied on unfiltered and filtered interference fringe pattern obtained using Michelson's interferometer without any external deformation. The extracted phase expected to show linear variations. The quality of extracted phase is measured using phase linearity error and root mean square (RMS) of phase noise for filtered and unfiltered fringe patterns. The RMS phase error and maximum deviation decreases for the filtered interference pattern as compared to unfiltered pattern. These results confirm that prior filtering of fringe pattern before applying the Fourier transform method significantly improves the phase quality, accuracy and reliability.

1 Introduction

Interferometric techniques have been identified as one of the most precise optical setup for determining displacement [1], deformations [2, 3] and refractive index [4]. The phase of the fringe pattern contains crucial quantitative information about these parameters. For example, take the case of the basic two beam interferometer. It is one of the most widely used optical setups due to its high sensitivity and simple configuration [5]. The fringe patterns obtained from it have information about the optical path difference of the interfering light waves. It has applications in areas such as metrology [6], imaging [7], all optical logic gates [8] and sensors [9–11]. Recent developments in Michelson interferometry include integrated photonic Michelson sensors [12, 13] and compact fringe counting displacement system [14]. Applications of interferometry range from Astronomy/Astrophysics [15] to thin film thickness measurement [16].

As mentioned earlier, the fringe patterns contain information about the optical path length difference between the two interfering waves. The change in the path difference may arise due to change in refractive index or small displacement/deformation of one of the mirrors. Extraction of phase information from fringes is very important for determining

*Corresponding author:pppadghan5@gmail.com

deformations [17], surface profiling [18], vibration analysis [19] and refractive index measurement [20, 21]. There are several techniques developed for fringe phase extraction [22–26]. Among these, the conventional phase shifting interferometry technique is known for precision phase measurement but requires multiple fringe patterns with known phase shifts and controlled phase shifting device [27–30]. The requirement of multiple images is a major limitation of phase-shifting interferometry compared with single-image methods. Dynamic systems, such as thermal deformation require rapid analysis of the temporally separated images. It is not feasible to use phase-shifting interferometry for measuring such thermal deformation/expansion. Hence, a single-image phase extraction method becomes necessary in this case.

Fourier transform method [31–35] is one such technique to extract phase information from a single frame. In the Fourier transform method, phase extraction is achieved by separating spatial carrier frequency from zeroth order and complex terms. By doing this, wrapped phase is obtained which has phase ambiguities ranging from $+\pi$ to $-\pi$. These ambiguities can be removed by using phase unwrapping algorithms [36, 37]. Fourier transform method proposed by Takeda et al. [31] is pretty straight forward and adopted by researchers for phase determination from the fringe pattern. In this method, the captured fringe pattern transformed in the frequency domain, where zeroth order and first order spectral components are separated from each other. Selecting any one of the first order sidebands using the bandpass filter and taking its inverse Fourier transform, we obtain the wrapped phase map. This method is very useful for instant phase extraction from a single image.

Despite the advantage of Fourier transform technique, its dependence on the accuracy of the frequency domain filtering [38–40], the presence of noise and high frequency spectral component in the pattern can result in difficulties while extracting phase information. Hence, it is important to carefully filter fringe patterns as well as frequency domain spectrum. The fringe patterns obtained from a two-beam interferometer are straight and uniformly spaced. Hence, without any deformation, the ideal phase distribution is expected to vary linearly along the direction perpendicular to the fringe pattern. To validate the method, it is important to observe the linear phase behaviour. This behaviour can be analysed from the amount of deviation between retrieved phase map and the linear phase fit, which can be used to determine whether any phase noise or errors arise during Fourier processing.

In this paper, Takeda's Fourier transform method is employed to extract the phase from single image of two beam interference fringe pattern. The band pass filter is applied to Fourier spectrum for selecting the first order spectral component for the removal of unwanted noise. Fourier transform method was implemented on the fringe patterns with and without filtering. Phase maps were extracted and phase quality was compared with the phase fit and assessed using quantitative error metrics such as RMS phase error and maximum phase deviation [39]. Results show that pre-filtering a fringe pattern before applying the Fourier transform improves the quality of the resulting phase maps.

2 Theoretical Background

The 2D fringe pattern can be expressed as [31],

$$I(x,y) = I_a(x,y) + I_b(x,y)\cos\left[2\pi(f_{0X}x + f_{0Y}y) + \varphi(x,y)\right] \tag{1a}$$

where, $I_b(x,y)$ is the background intensity, $I_a(x,y)$ is Amplitude, $\varphi(x,y)$ phase and f_0 is spatial frequency carrier.

$$\Rightarrow I(x,y) = I_a(x,y) + I_b(x,y)\left[\frac{e^{i(2\pi(f_{0X}x+f_{0Y}y)+\varphi(x,y))} + e^{-i(2\pi(f_{0X}x+f_{0Y}y)+\varphi(x,y))}}{2}\right] \quad (1b)$$

$$\left[\because \cos\theta = \frac{e^{i\theta} + e^{-i\theta}}{2}\right]$$

$$\Rightarrow I(x,y) = I_a(x,y) + \frac{1}{2} I_b(x,y) e^{i\phi(x,y)}.e^{2\pi i(f_{0X}x+f_{0Y}y)} + \frac{1}{2} I_b(x,y) e^{-i\phi(x,y)}.e^{-2\pi i(f_{0X}x+f_{0Y}y)} \quad (1c)$$

$$I(x,y) = I_a(x,y) + P(x,y).e^{2\pi i(f_{0X}x+f_{0Y}y)} + P^*(x,y).e^{-2\pi i(f_{0X}x+f_{0Y}y)} \quad (2)$$

where,

$$P(x,y) = \frac{1}{2} I_b(x,y) e^{i\varphi(x,y)} \quad (3)$$

Taking Fourier transform of Eq. (2), we get,

$$F\left[I(x,y)\right] = F\left[I_a(x,y)\right] + F\left[P(x,y).e^{2\pi i(f_{0X}x+f_{0Y}y)}\right] + F\left[P^*(x).e^{-2\pi i(f_{0X}x+f_{0Y}y)}\right] \quad (4a)$$

Using the shifting theorem,

$$I(f_X, f_Y) = I_A(f_X, f_Y) + P(f_X - f_{X0}, f_X - f_{Y0}) + P^*\left[-(f_X + f_{X0}), -(f_X + f_{Y0})\right] \quad (4b)$$

Now taking log of Eq. (3) we get,

$$\log[P(x,y)] = \log\left[\frac{1}{2} I_b(x,y)\right] + \log\left[e^{i\varphi(x,y)}\right] \quad (5a)$$

$$= \log\left[\frac{1}{2} I_b(x,y)\right] + i\varphi(x,y).\log e \quad (5b)$$

$$\log[P(x,y)] = \log\left[\frac{1}{2} I_b(x,y)\right] + i\varphi(x,y) \qquad \because (\log e = 1) \quad (5c)$$

Here, $\log\left[\frac{1}{2} I_b(x,y)\right]$ represent amplitude and $i\varphi(x,y)$ represents phase of the fringe pattern.

3 Theoretical Background

Fig. 1 shows the two-beam interferometer set up in which light from the diode laser was divided into two halves using a beam splitter. One beam goes in the direction of the mirror 1 and other is incident on mirror 2. Upon reflection, both beams superpose to give an interference pattern which can be visualized and saved using a digital camera attached to a computer. The interference fringe pattern shows occurrence of constructive interference or destructive interference depending on whether the superposing waves are in phase or out of phase with each other. In the intermediate cases, the total electric vector displacement is given by the vector resultant, and the intensity is proportional to the square of resultant displacement amplitude. The fringe pattern obtained from this setup was analysed using the Fourier transform.

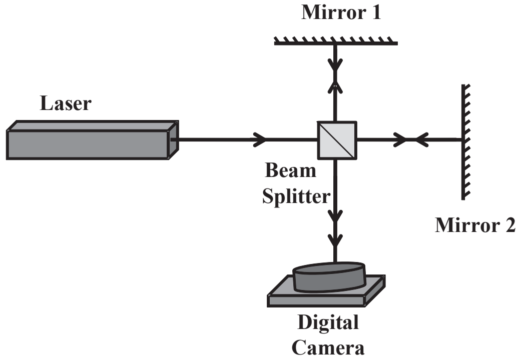

Fig. 1. Schematics of two beam interferometer

4 Results and Discussion

The interference fringe pattern obtained using the experimental setup of the two-beam interferometer is shown in Fig. 2(a). These images were then processed using frequency-domain filtering. Figure 2(b) shows the filtered fringe pattern, which exhibits reduced noise and smoother fringes compared to Fig. 2(a).

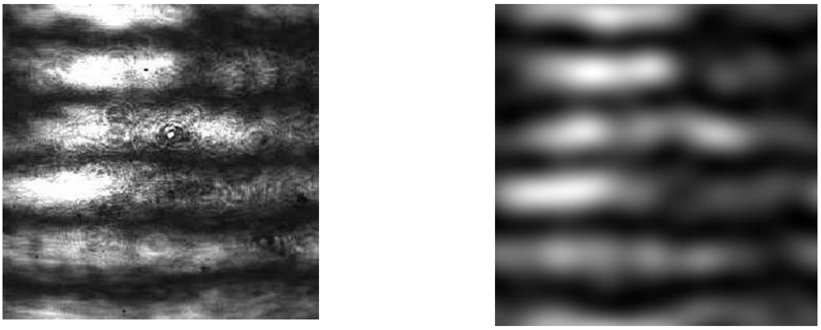

(a) (b)

Fig. 2. Interference fringe patterns- (a) Experimental and (b) Filtered

These interference fringe patterns were then transformed into frequency domain using fast Fourier transform which gives us the frequency domain spectrum. Fig. 3 shows 2D and 3D frequency spectrum of unfiltered fringe pattern. The spectrum shows three peaks which are expected from Eq. (4) containing the background intensity term at the centre and two first order sidebands that represent the modulated phase map. However, the Fourier domain contains an ample amount of noise which can affect the phase map.

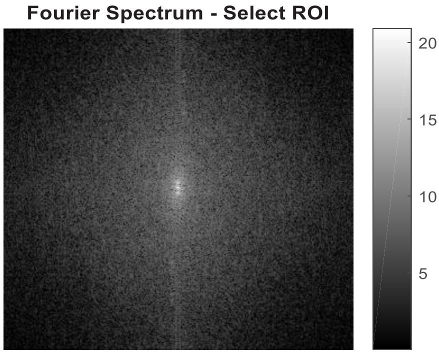

(a)

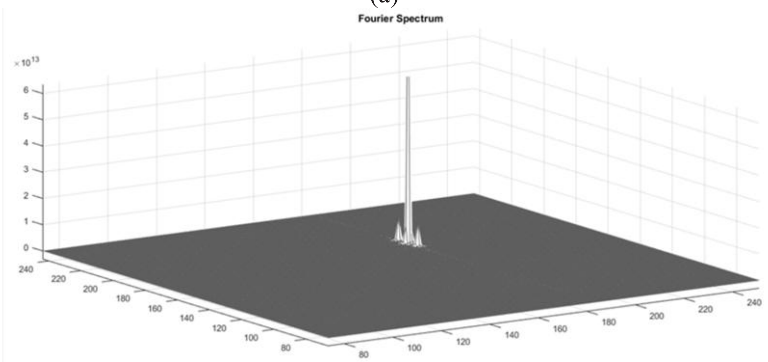

(b)

Fig. 3. Fourier spectrum of transformed fringe patterns- (a) 2D and (b) 3D frequency plot without filtering

Fig. 4 shows the 2D and 3D frequency domain spectrum of fringe pattern after Fourier domain band pass filtering. As we can see from the plot, the central DC term and noise has been removed from frequency domain. Now we can implement Fourier transform to separate out single first order frequency term from it.

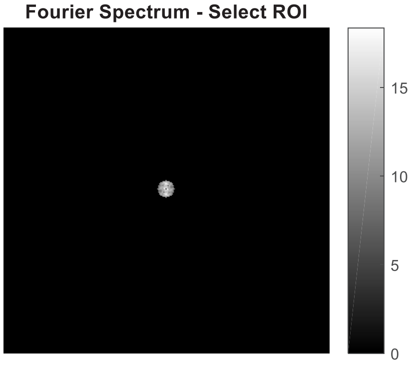

(a)

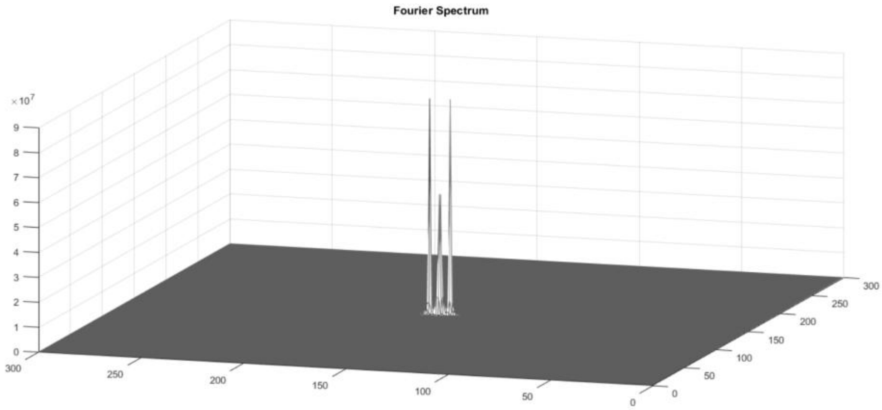

(b)

Fig. 4. Fourier spectrum of transformed fringe patterns- (a) 2D and (b) 3D frequency plot after filtering

Band pass filter is applied to isolate the first order spectral lobe. After isolating, it is then shifted to the centre. After an inverse Fourier transform, the image is then transformed back to spatial domain which later can give rise to wrapped phase maps as shown in Fig. 5. As we can see from Fig. 5 (a), the wrapped phase map obtained from unfiltered fringe pattern contains irregular phase jumps while filtered fringe pattern gives smooth wrapped phase map as shown in Fig. 5(b). The wrapped phase map includes discontinuities from $+\pi$ to $-\pi$.

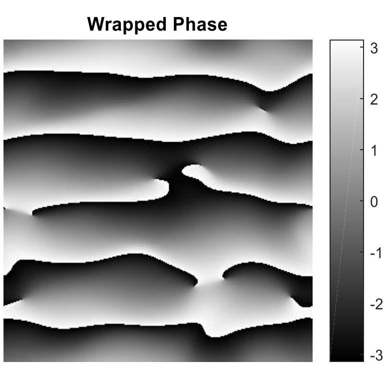

(a)

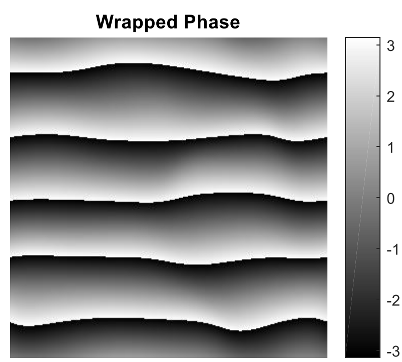

(b)

Fig. 5. Wrapped phase maps of fringe patterns (a).Without Filter and (b). After Filtering

To extract phase information from it, we need to unwrap this wrapped phase map by 2D phase unwrapping algorithm [37]. Fig. 6 shows unwrapped phase maps of (a) unfiltered and (b) filtered fringe patterns. The unwrapped phase map of unfiltered fringe pattern shown in Fig. 6 (a) consists of artifacts attributed to noise present in the original image, while filtered fringe pattern gives a smooth phase map as shown in Fig. 6 (b).

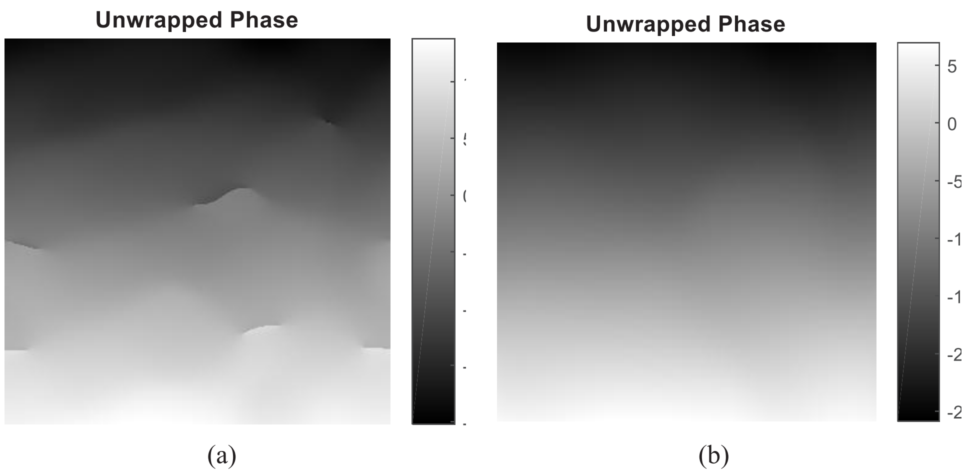

Fig. 6. Unwrapped phase maps of fringe pattern (a).Without Filter and (b). After Filtering

Fig. 7 (a) shows clear deviations along the linear phase fit for the unfiltered fringe pattern. This is because of unwanted spectral components and noise. Whereas, Fig. 7 (b) shows the phase map with reduced deviations after applying frequency domain filtering. This confirms the efficiency of frequency domain filtering for accurate phase extraction.

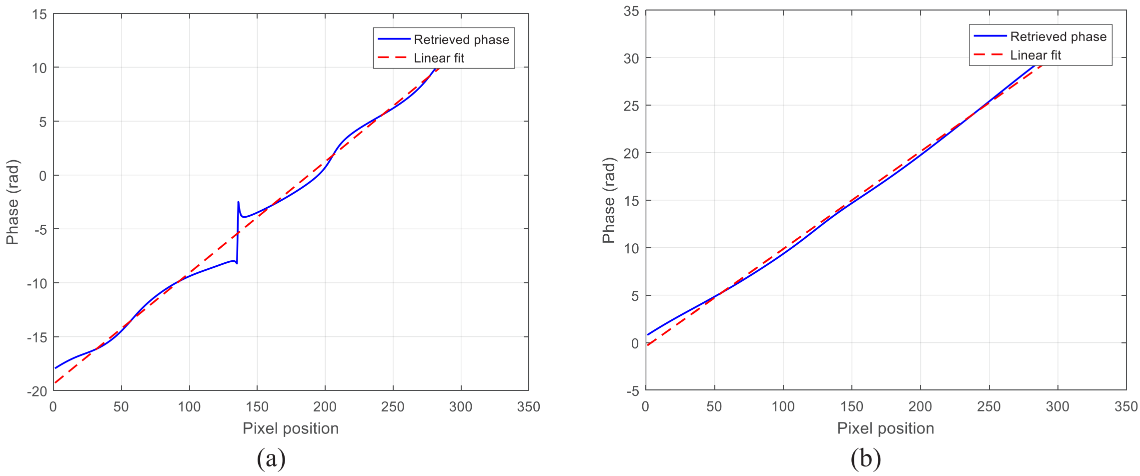

Fig. 7. Retrieved phase plot of fringe pattern (a) without filtering and (b) with filtering.

RMS phase error, Max phase error and 2D RMS phase noise of unfiltered and filtered unwrapped phase map was quantitatively reported in Table 1.

Table 1. Quantitative phase error and phase noise of unwrapped phase map.

Sr. No	Type of fringe pattern	RMS phase error	Max phase error	2D RMS phase noise
1	**Unfiltered**	0.7205 rad	2.8741 rad	9.3864 rad
2	**Filtered**	0.4506 rad	1.1008 rad	9.3704 rad

The effect of Fourier domain filtering on the unwrapped phase map quality was evaluated using phase error metrics. The RMS phase error reduced from 0.7205 rad to 0.4506 rad after filtering, which gives 37% improvement. The maximum phase deviation was reduced from 2.8741 rad to 1.1008 rad i.e. 62% reduction. These results show that Fourier domain filtering efficiently reduces noise and high frequency distortion which gives an improved phase linearity and enhanced reliability for phase extraction from single interference fringe pattern.

5 Conclusions

Phase information was extracted successfully from single fringe pattern using the Fourier transform method introduced by Takeda et. al [31]. Pre-filtering of fringe pattern plays an important role in improving phase quality besides making it noise free. Error analysis comparison demonstrated reduction in maximum phase deviation by approximately 62% and 37% in RMS phase error respectively. Our results confirm better accuracy in extracting phase from single fringe pattern obtained from two beam interferometer.

Authors acknowledge with gratitude the computational facilities offered by the Principal, Shri Shivaji Science and Arts College Chikhli, Dist. Buldana and Jijamata Mahavidyalay, Buldhana. The authors are thankful to the Head of the Physics Department of SGB Amravati University Amravati for offering the necessary resources that made this research possible.

References

1. A.T. Hoang, T.T. Vu, D.Q. Pham, T.T. Vu, T.D. Nguyen, V.H. Tran, High precision displacement measuring interferometer based on the active modulation index control method. Measurement 214, 112819 (2023). https://doi.org/10.1016/j.measurement.2023.112819
2. V.V. Balandin, D.A. Mansfeld, K.V. Mineev, V.V. Parkhachev, R.M. Rozental, A.V. Vodopyanov, Measuring fast mechanical deformation with micrometer precision based on millimeter wave interferometry. J. Infrared Millim. Terahertz Waves 45, 749–764 (2024). https://doi.org/10.1007/s10762-024-01006-8
3. T.A. Berfield, J.K. Patel, R.G. Shimmin, P.V. Braun, J. Lambros, N.R. Sottos, Micro- and nanoscale deformation measurement of surface and internal planes via digital image correlation. Exp. Mech. 47, 51–62 (2007). https://doi.org/10.1007/s11340-006-0531-2

4. Y.J. Kim, P.M. Celliers, J.H. Eggert, A. Lazicki, M. Millot, Interferometric measurements of refractive index and dispersion at high pressure. Sci. Rep. 11, 5610 (2021). https://doi.org/10.1038/s41598-021-84883-6
5. K.G. Libbrecht, E.D. Black, A basic Michelson laser interferometer for the undergraduate teaching laboratory demonstrating picometer sensitivity. Am. J. Phys. 83, 409–417 (2015). https://doi.org/10.1119/1.4901972
6. D.G. Abdelsalam, B. Yao, Interferometry and its applications in surface metrology, in Optical Interferometry (InTech Open, 2017). https://doi.org/10.5772/66275
7. A. Faridian, D. Hopp, G. Pedrini, U. Eigenthaler, M. Hirscher, W. Osten, Nanoscale imaging using deep ultraviolet digital holographic microscopy. Opt. Express 18, 14159–14164 (2010). https://doi.org/10.1364/OE.18.014159
8. P.P. Padghan, K.M. Alti, Experimental realization of multiple all optical universal logic gates using array illuminator. Int. J. Pure Appl. Res. Eng. Technol. 2, 238–245 (2014)
9. J. Cubik, S. Kepak, A. Liner, M. Papes, T. Kajnar, O. Zboril, J. Jaros, V. Vašinek, Optical vibration sensor based on Michelson interferometer arrangement with polarization-maintaining fibers, in Fiber Optic Sensors and Applications XI (SPIE, 2014), p. 90980I. https://doi.org/10.1117/12.2050528
10. J. Shen, D. Donnelly, S. Chakravarty, Integrated photonic slow light Michelson interferometer biosensor, in Integrated Optics: Devices, Materials, and Technologies XXVII, ed. by S.M. García-Blanco, P. Cheben (SPIE, 2023), p. 85. https://doi.org/10.1117/12.2650514
11. L. Yuan, J. Yang, Z. Liu, J. Sun, In-fiber integrated Michelson interferometer. Opt. Lett. 31, 2692–2694 (2006). https://doi.org/10.1364/OL.31.002692
12. Z. Yue, L. Feng, W. Feng, UiO-66 metal-organic framework integrated Michelson interferometer for fluoride-ion detection. Opt. Fiber Technol. 70, 102885 (2022). https://doi.org/10.1016/j.yofte.2022.102885
13. Y. Guo, L. Zhou, L. Guo, W. Jiang, J. Du, X. Chen, H. Wang, X. Bao, Y. Du, J. Qu, Y. Zhong, R. Zhou, Y. Wu, Y. Guo, W. Chen, Integrated photonics for space communication and sensing. J. Phys. Photonics 7, 042001 (2025). https://doi.org/10.1088/2515-7647/ade64b
14. K.-S. Isleif, G. Heinzel, M. Mehmet, O. Gerberding, Compact multifringe interferometry with subpicometer precision. Phys. Rev. Appl. 12, 034025 (2019). https://doi.org/10.1103/PhysRevApplied.12.034025
15. I. Guidi, B. Melchiorri, F. Melchiorri, V. Natale, A Michelson interferometer for astronomical applications. Infrared Phys. 18, 267–273 (1978). https://doi.org/10.1016/0020-0891(78)90129-X
16. H.M. Shabana, Determination of film thickness and refractive index by interferometry. Polym. Test. 23, 695–702 (2004). https://doi.org/10.1016/j.polymertesting.2004.01.006
17. P.P. Padghan, K.M. Alti, Quantification of nanoscale deformations using electronic speckle pattern interferometer. Opt. Laser Technol. 107, 72–79 (2018). https://doi.org/10.1016/j.optlastec.2018.05.019
18. H. Liu, W.H. Su, K. Reichard, S. Yin, Calibration-based phase-shifting projected fringe profilometry for accurate absolute 3D surface profile measurement. Opt. Commun. 216, 65–80 (2003). https://doi.org/10.1016/S0030-4018(02)02290-3
19. Y. Fu, G. Pedrini, W. Osten, Vibration measurement by temporal Fourier analyses of a digital hologram sequence. Appl. Opt. 46, 5719–5727 (2007). https://doi.org/10.1364/AO.46.005719

20. A. Abou Khalil, W. Gebremichael, Y. Petit, L. Canioni, Refractive index change measurement by quantitative microscopy phase imaging for femtosecond laser written structures. Opt. Commun. 485, 126731 (2021). https://doi.org/10.1016/j.optcom.2020.126731
21. K. Zhang, O. Sasaki, S. Choi, S. Luo, T. Suzuki, J. Pu, Measurement of phase refractive index directly from phase distributions detected with a spectrally resolved interferometer. Appl. Opt. 60, 10009 (2021). https://doi.org/10.1364/AO.438267
22. G.H. Kaufmann, Phase measurement in temporal speckle pattern interferometry using the Fourier transform method with and without a temporal carrier. Opt. Commun. 217, 141–149 (2003). https://doi.org/10.1016/S0030-4018(03)01160-X
23. Y. Xia, S. Xiangyi, Y. Qifeng, F. Sihua, Direct ESPI phase estimating from only two interferograms. Opt. Commun. (2013). https://doi.org/10.1016/j.optcom.2012.10.060
24. A. Patil, P. Rastogi, Phase determination in holographic Moiré in presence of nonsinusoidal waveforms and random noise. Opt. Commun. 257, 120–132 (2006). https://doi.org/10.1016/j.optcom.2005.07.026
25. B. Pan, K. Li, A fast digital image correlation method for deformation measurement. Opt. Lasers Eng. 49, 841–847 (2011). https://doi.org/10.1016/j.optlaseng.2011.02.023
26. T. Bothe, J. Burke, H. Helmers, Spatial phase shifting in electronic speckle pattern interferometry: minimization of phase reconstruction errors. Appl. Opt. 36, 5310–5316 (1997). https://doi.org/10.1364/AO.36.005310
27. O. Elijah, G.K. Rurimo, P.M. Karimi, Optical phase shift measurements in interferometry. Int. J. Optoelectr. Eng. 3, 13–18 (2013). https://doi.org/10.5923/j.ijoe.20130302.01
28. X. Chen, M. Gramaglia, J.A. Yeazell, Phase-shifting interferometry with uncalibrated phase shifts. Appl. Opt. 39, 585–591 (2000). https://doi.org/10.1364/AO.39.000585
29. C. Joenathan, Phase-measuring interferometry: new methods and error analysis. Appl. Opt. 33, 4147–4155 (1994). https://doi.org/10.1364/AO.33.004147
30. K. Creath, Phase-shifting speckle interferometry. Appl. Opt. 24, 3053–3058 (1985). https://doi.org/10.1364/AO.24.003053
31. M. Takeda, H. Ina, S. Kobayashi, Fourier-transform method of fringe-pattern analysis for computer-based topography and interferometry. J. Opt. Soc. Am. 72, 156–160 (1982). https://doi.org/10.1364/JOSA.72.000156
32. T. Kreis, Digital holographic interference-phase measurement using the Fourier-transform method. J. Opt. Soc. Am. A 3, 847–855 (1986). https://doi.org/10.1364/JOSAA.3.000847
33. J.T. Judge, C. Quan, P.J. Bryanston-Cross, Holographic deformation measurements by Fourier transform technique with automatic phase unwrapping. Opt. Eng. 31, 533–543 (1992). https://doi.org/10.1117/12.56092
34. J.B. Liu, P.D. Ronney, Modified Fourier transform method for interferogram fringe pattern analysis. Appl. Opt. 36, 6231–6241 (1997). https://doi.org/10.1364/AO.36.006231
35. X. Gao, S. Wu, L. Yang, Dynamic measurement of deformation using Fourier transform digital holographic interferometry, in Proceedings of SPIE 8916, 891617 (2013). https://doi.org/10.1117/12.2035889
36. J. Cheng, Y. Mei, B. Liu, J. Guan, X. Liu, E.X. Wu, Q. Feng, W. Chen, Y. Feng, A novel phase-unwrapping method based on pixel clustering and local surface fitting with

application to Dixon water–fat MRI. Magn. Reson. Med. 79, 515–528 (2018). https://doi.org/10.1002/mrm.26647

37. M.A. Herráez, D.R. Burton, M.J. Lalor, M.A. Gdeisat, Fast two-dimensional phase-unwrapping algorithm based on sorting by reliability following a noncontinuous path. Appl. Opt. 41, 7437–7444 (2002). https://doi.org/10.1364/AO.41.007437
38. Z. Gao, Q. Chang, Y. Deng, W. Liu, P. Ma, P. Zhou, L. Si, Tilt noise extraction method based on Fourier transform and fitting of 2D images. Opt. Commun. 577, 131372 (2025). https://doi.org/10.1016/j.optcom.2024.131372
39. Y. Mejía, Noise reduction in the Fourier spectrum of Hartmann patterns for phase demodulation. Opt. Commun. 281, 1047–1055 (2008). https://doi.org/10.1016/j.optcom.2007.10.091
40. K. Qian, Two-dimensional windowed Fourier frames for noise reduction in fringe pattern analysis. Opt. Eng. 44, 075601 (2005). https://doi.org/10.1117/1.1948107